




HASP Student Payload Application for 2023

Payload Title: The Electron Spectrometer Telescope (EST)		
Institution: McMaster University		
Payload Class (Enter SMALL, or LARGE): LARGE		Submit Date: January 6, 2023
<p>Project Abstract: Energetic electrons within Earth's radiation belts often undergo scattering causing them to interact with the atmosphere. In doing so, the energetic particles produce strange nitrogen and hydrogen atoms which catalytically deplete the ozone layer. The effects and impact of energetic electron precipitation are not well understood due to a lack of high-resolution angular electron spectra. To address this measurement gap, we are developing the Pitch RESolving Spectroscopy for Electron Transport (PRESET) mission. PRESET will be composed of the Electron Spectrometer Telescope (EST), which when combined with a magnetometer will be able to measure precipitating electron spectra with high angular resolution. The EST will be capable of distinguishing between electrons and protons while rejecting events from gamma rays, muons, and heavier ions. A balloon flight will allow for the EST instrument to be tested in a near space environment measuring primary and secondary galactic cosmic rays and their secondary particles. Successful mechanical and electrical designs from the HASP 2017, 2018, and 2021 missions will be used with minor modifications to accelerate the development process and allow the team to focus on ensuring an operational instrument is completed for HASP 2023 capable of collecting, processing, and transmitting spectral data.</p>		
Team Name: PRESET-EST Team		Team or Project Website:
Student Leader Contact Information:		Faculty Advisor Contact Information:
Name:	Benjamin Dyer	Dr. Andrei Hanu
Department:	Physics and Astronomy	Physics and Astronomy
Mailing Address:	1280 Main Street West	1280 Main Street West
City, State, Zip code:	Hamilton, Ontario, Canada, L8S 4K1	Hamilton, Ontario, Canada, L8S 4K1
e-mail:	dyerbm@mcmaster.ca	hanua@mcmaster.ca
Telephone:	289-828-5508	519-708-3552
<p>The signature below indicates that the student lead and faculty advisor have read and understood the HASP CFP and Student Payload Interface manual, commit to providing the required HASP deliverables by the indicated due dates and agree to respond to HASP management inquiries in a timely manner.</p>		
Commitment Signature:		

Flight Hazard Certification Checklist

NASA has identified several classes of material as hazardous to personnel and/or flight systems. This checklist identifies these documented risks. Applying flight groups are required to acknowledge if the payload will include any of the hazards included on the list below. Simply place an (x) in the appropriate field for each hazard classification. **Note:** Certain classifications are explicitly banned from HASP and the remaining hazards will require additional paperwork and certifications. If you intend to include one of the hazards, you must include detailed documentation in section 3.8 of the application as required by the HASP Call for Payloads.

This certification must be signed by both the team faculty advisor and the student team lead and included in your application immediately following the cover sheet form.

Hazardous Materials List		
Classification	Included on Payload	Not Included on Payload
RF transmitters		X
High Voltage	X	
Lasers (Class 1, 2, and 3R only) Fully Enclosed		X
Intentionally Dropped Components		X
Liquid Chemicals		X
Cryogenic Materials		X
Radioactive Material		X
Pressure Vessels		X
Pyrotechnics		X
Magnets less than 1 Gauss*		X
UV Light		X
Biological Samples		X
Non-Rechargeable Batteries		X
Rechargeable Batteries		X
High intensity light source		X

* Magnets greater than 1 gauss are banned.

Student Team Leader Signature: 

Faculty Advisor Signature: 

1. Payload Description

1.1 Payload Scientific / Technical Background

Relativistic electrons are trapped in the outer Van Allen radiation belt and the electron flux decreases rapidly during the main phase of the magnetic storms, and then increases during the storms' recovery phase. As the time-dependent variation of the electron flux is coupled to the magnetic storms, collecting the electron flux spectrum data and analyzing its time dependence is of great importance for understanding the physics that governs the electron flux variation. Additionally, electrons absorbed by the atmosphere produce nitric and hydrogen oxides which deplete the ozone at high latitudes. Currently, the energy region from 2-7 MeV is missing from the spectrometers operating in LEO, so developing a spectrometer to cover this missing energy region is of great importance. To this end, we are developing an electron spectrometer consisting of multiple silicon charged particle detectors arranged in a telescopic geometry.

Following our highly successful NEUtron DOSimetry & Exploration (NEUDOSE) CubeSat mission [1-4], which will launch in March 2023, McMaster University is proposing its next CubeSat mission that will study the dynamics of electrons in the Earth's magnetosphere. With this next mission, we aim to measure the pitch-angle distribution of energetic electrons, which are trapped within the Van Allen radiation belts and often exhibit dramatic and highly dynamic changes during geomagnetic storms. Some of these storms result in the loss of electrons from the Van Allen radiation belts through atmospheric absorption, but the intensity, timescale, and effects from the loss of electrons is currently unknown. To address this knowledge gap, we propose the Pitch RESolving Spectroscopy for Electron Transport (PRESET) CubeSat mission. PRESET is a 3U CubeSat that will carry two scientific instruments into a preferred high-inclination low-Earth orbit (LEO) to measure the angle and time-dependent flux of electrons with kinetic energies ranging from 0.3 – 7 MeV. The first instrument is a highly collimated Electron Spectrometer Telescope (EST) that will measure the energy and arrival time of electrons incident upon the instrument's acceptance angle. The second instrument is a tri-axial MAGnetometer (MAG) that will be mounted at the end of a 1-meter deployable boom and used to measure the strength and direction of the local magnetic field. The data from these two instruments will be combined with attitude and pointing knowledge from the PRESET CubeSat, enabling us to measure the angle and time-dependent flux of electrons incident upon the spacecraft.

1.1.1 Mission Statement

The payload instrument EST, upon integration with MAG and the rest of PRESET will measure the spectrum of energetic electrons which interact with Earth's atmosphere.

This is accomplished by measuring the angle between particle velocity and the local magnetic field vector, called pitch angle. If the pitch angle is sufficiently small, the electron is within the loss cone and will interact with the atmosphere. These interactions remove electrons from the radiation belts and drive production of nitric and hydrogen oxides (NO_x, HO_x) in the upper atmosphere.

While it has been established that these chemicals catalytically destroy the ozone layer, the strength and frequency of the effects are not agreed upon due to a lack of reliable data. The final data product will be high quality loss cone spectrums, enabling accurate medium energy electron precipitation data to be used in NO_x and HO_x production simulations, and furthering understanding of atmospheric-ionospheric-magnetospheric interactions.

1.1.2 Mission Background and Justification

The Van Allen belts are regions of radiation surrounding the Earth, composed primarily of energetic electrons or protons and a much smaller fraction of heavier ions. Measurement of the spatial and temporal particle flux distributions have always been of great interest due to the negative health effects of energetic particles, strong coupling to space weather, the existence of ‘killer’ electrons which can disable satellites and understanding atmospheric-ionospheric-magnetospheric interactions (AIM) [5][6]. In more recent years, the loss of Van Allen belt electrons to the upper atmosphere has been of great interest because of the potential link to global warming caused by the depletion of the northern and southern ozone layers.

Research over the past decade has shown that precipitation of medium energy electrons (MEE), that is electrons within the loss cone, leads to production of nitric (NO_x) and hydrogen oxides (HO_x). In turn, these chemicals deplete atmospheric ozone through catalytic reactions [7]. Ozone depletion contributes directly and indirectly to climate change by altering atmospheric circulation patterns. This leads to changes in sea surface temperatures, weather patterns, weather conditions, and increased wild-fire risks [8-12]. While research into these effects has focused on the southern hemisphere, similar, but lower intensity effects also exist in the northern hemisphere. The most severe effects are expected during the polar winter when a lack of sunlight and low wind velocities leads to NO_x and HO_x lifetimes on the order of months [12].

Ozone loss due to NO_x and HO_x production has been predicted using multiple models with varying results. Predictions from the Canadian Middle Atmosphere Model suggest a 60% and 80% ozone loss due to MEE in the northern and southern hemisphere, respectively [13]. Application of the Thermosphere Ionosphere Mesosphere General Circulation Model and the Solar Climate Ozone Links model, suggests a 27% and 33% decrease in ozone, respectively [14][15]. Opposing these models, analysis using the HAMMONIA model suggests no significant effect on ozone due to MEE precipitation [16]. A large factor in discrepancies between models is a lack of accurate MEE precipitation data (i.e., electron spectrum data within the loss cone) leading models to be simulated using approximated data sets with significant uncertainty [17][18].

Measurement of the pitch angle distribution began with the Energetic Particle, Composition, and Thermal Plasma (ECT) suite on board the Van Allen Probes (VAPs) [19]. The VAPs launched in 2012, taking the first detailed measurements of the electron pitch angle density with a resolution of 10 degrees [20]. Since the loss cone decreases to less than 5 degrees quickly with altitude, the geostationary transfer orbit of the VAPs resulted in directional spectrum measurements containing but not entirely within the loss cone [19]. Following the decommissioning of the VAPs, the ARASE mission began measuring the pitch angle densities of electrons in the energy range of 0.07-2 MeV. With a maximum angular resolution of 4 degrees, ARASE can take one spectrum measurements completely within the loss cone for energies from 70 keV to 1 MeV. When at non-equatorial latitudes the loss cone increases slightly allowing an additional spectrum containing the

edge and region just outside the loss cone [21][22]. The PRESET mission will measure the electron pitch angle density with an angular resolution of <10 degrees across an energy range of 0.3-7MeV. These requirements fill a gap in the energy spectrum since previous LEO missions have measured up to a maximum of 6MeV.

Although the loss cone information cannot be obtained at HASP altitudes, the radiation environment at HASP's float altitude provided an excellent opportunity to test and verify the functionality and performance of the EST. Sources are primary and secondary galactic cosmic rays at the balloon float altitude. Collisions of primary Galactic Cosmic Rays (GCRs) with nuclei in the upper atmosphere result in a shower of gamma and lighter hadronic particles including pions, muons, electrons, and neutrinos, which are secondary GCR particles. From the EXPACS (EXcel-based Program for calculating Atmospheric Cosmic-ray Spectrum) database, the expected atmospheric cosmic-rays spectrum at HASP float altitude and latitude can be obtained. The EST is designed to measure electrons and protons from a complex radiation field using coincidence techniques (more details in section 1.2). Within the instrument detection range, various radiation including photons, electrons, protons, muons and helium ions will be detected. The EST instrument shall be able to identify and exclude gamma, muon, and heavy ion events in real time.

With a flight on HASP, we will expose the EST to a near space like radiation environment, enabling us to characterize the instrument performance and determine the optimum instrument parameters for the future LEO flights.

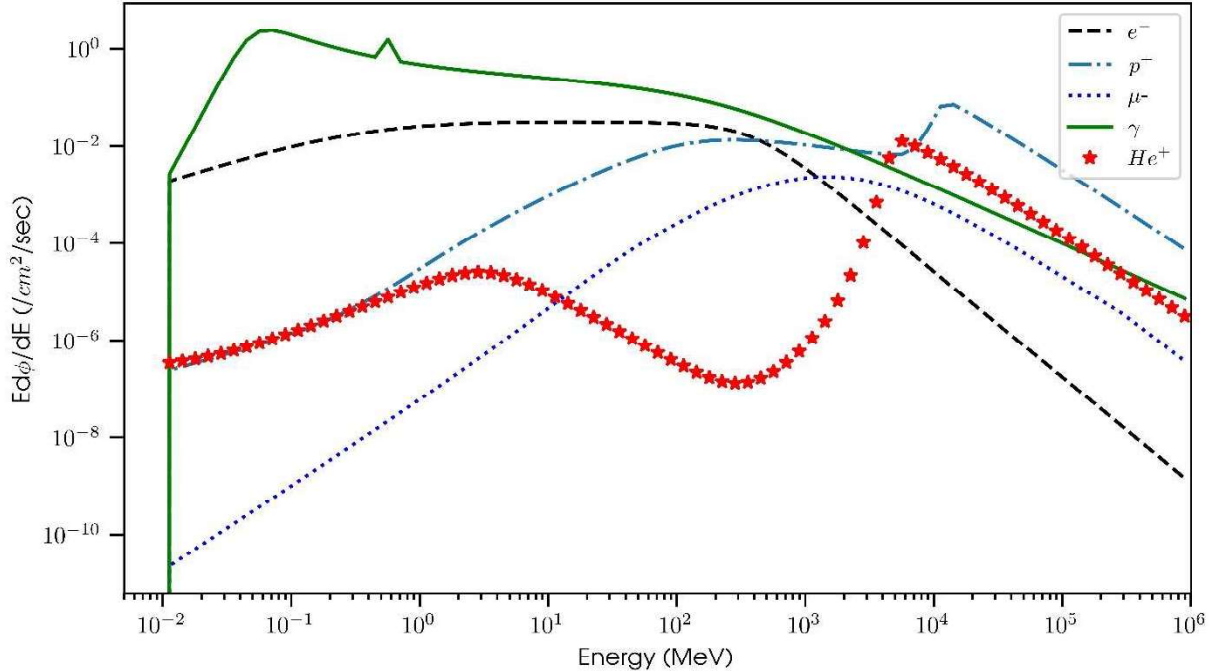


Figure 1 - Atmospheric cosmic ray spectrum of selected radiation types at HASP altitude (36 km, 5.3 g cm⁻²) and latitude (34.5N, 104W) [23]

1.1.3 Mission Objectives

For the HASP 2023 opportunity, a preliminary version of PRESET will be flown consisting of the electron spectrometer, communications module, and flight computer. The mission objectives are as follows:

- Demonstrate stable operation of the EST
- Collect both an electron and proton spectrum every 5 minutes
- Validate spectrums with Geant4 cosmic ray shower simulations
- Demonstrate active shutter during launch, landing, and when sun pointing
- Demonstrate effectiveness of thermal control systems on the spectrometer detectors
- Validate thermal range functionality in TVAC

1.1.4 Scientific Relevance to the HASP Platform

The HASP platform will provide an opportunity to test PRESET's primary payload, EST, in a near-space environment. Through the HASP platform, the instrument will be exposed to a similar environment to LEO, validating thermal and mechanical design. The effectiveness of the thermal design is of particular importance since temperature variations are expected to significantly affect system noise and therefore data product quality. Additionally, an actuatable shutter will be tested to block the entrance to the detector during launch, landing, and when the sun is within the instrument's viewing angle.

1.2 Payload Systems and Principle of Operation

The Electron Spectrometer Telescope (EST) is the primary payload of the PRESET CubeSat that we want to test on HASP 2023. EST can measure both the energy and arrival time of electrons that are incident upon the acceptance angle of the instrument. To accomplish this, the EST instrument consists of a stack of fully depleted silicon detectors which are arranged in a telescope configuration and individually connected to front end electronics that are readout simultaneously and in real-time. A rendering showing the notional design of the EST instrument is shown in Figure 2. As an advanced radiation spectrometer, the EST enables the ability to accurately measure electron flux by eliminating the contamination from gamma-rays, protons, or other ions. Electrons, and other charged particles, that enter the EST instrument through the collimator will interact with multiple silicon detectors consecutively. Gamma-rays, however, are unlikely to interact with consecutive detectors and can therefore be filtered using appropriate detector coincidence logic. For protons and ions, due to characteristic differences in the energy deposition mechanism, the detector responses would behave differently compared to electrons which can help us to distinguish and exclude the non-interesting events.

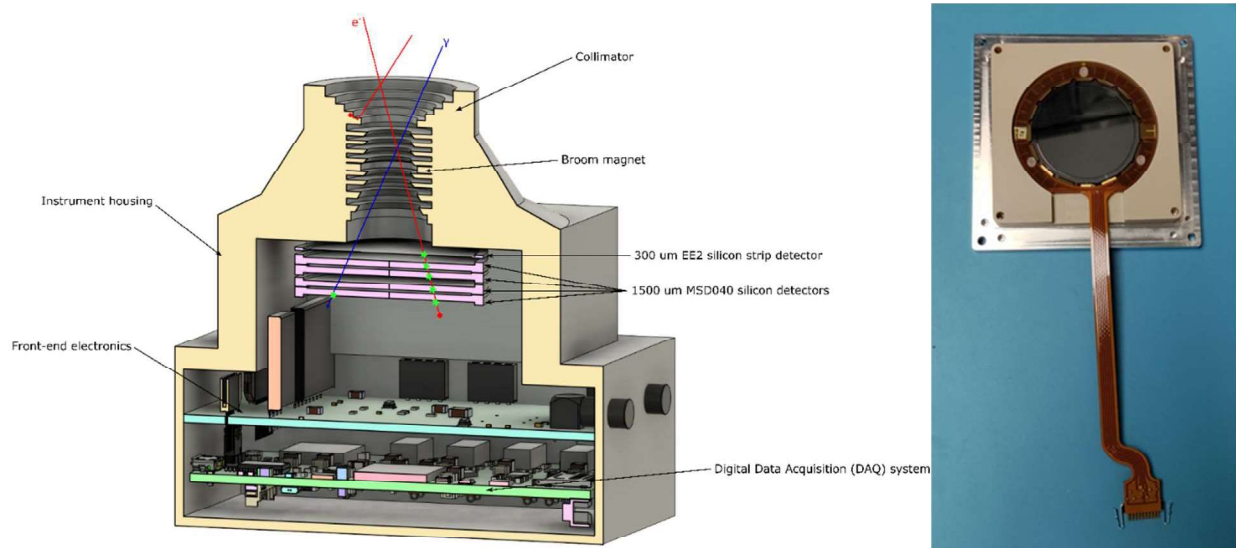


Figure 1 – Left: Rendering of the proposed EST instrument depicting the stack of silicon detectors, the mechanical housing with the narrow collimator, as well as the front end and data acquisition electronics. Right: Image of a 1500 μm thick silicon pad detector (model MSD040), that we have already purchased from Micron Semiconductor Ltd and using to construct a prototype version of the EST instrument.

1.3 Major System Components

1.3.1 Silicon Detector Stack

The EST instrument uses ΔE -E technique to identify charged particles and simultaneously measure their energy, arrival time, and angle of incidence. The detector stack consists of a 500 μm thick silicon strip detector (model EE2) at the entrance and four 1500 μm thick silicon pad detectors (model MSD040) from Micron Semiconductor Ltd, UK. EE2 is a silicon strip detector that contains 40 strips that will be triggered by electrons entering the detector. In this configuration, the incidence angle of electrons is calculated based on the hitting position of the strip together with the given collimator dimension. MSD040 is a n-type totally depleted ion implanted silicon detector with an active area diameter 40 mm and are 1500 μm thickness for ΔE -E energy measurement. Thick silicon detectors are paired based on electric characteristics and biased in cathode-to-cathode configuration, which avoids large voltage differences between two adjunct detector surfaces.

1.3.2 Collimator

A knife-edge disk-loaded collimator opening along the z-axis is on top of the silicon detector stack. Monte Carlo simulations (MCNP and GEANT4) are performed to model the collimator dimension in order to achieve desired geometric factor (the gathering power) and optimize for scattering, cut-off energies and ray tracing. The collimator needs to be a hard aperture for high energy particles which requires careful consideration calculation on material selection and disk thickness. Tantalum is the current top candidate for the collimator rings, but given the mechanical difficulties, phosphor-bronze and tungsten alloys may be used instead when precision comes to be important. Aluminum spacers are used between collimator rings to reduce

back scattering. At the back of the collimator, a beryllium window is fixed in place on a disk to provide a light-tight seal and filter very low energy particles to prevent saturation of the system.

1.3.3 Detector Housing

For mechanical resilience, the silicon detectors are mounted in an aluminum housing that shields the detector stack from particles entering from five sides. Charged particles are allowed to enter the silicon stack, and be measured, through a long and narrow collimator mounted to the housing. Front-end electronics and data acquisition module are mounted inside the housing. An inner vault with a thin tantalum or tungsten layer is inside the aluminum housing to suppress the effect of energetic penetrating particles, X-ray and secondary radiations.

1.3.4 EST Front-end Electronics

The EST front-end electronics contains a High Voltage Module (HVM) and a Front-end Amplification Module (FAM). There are two types of silicon detector with different thickness which require two sets of power supply to ensure the correct fully depletion voltage is applied to the detectors. The HVM contains high voltage supplies that meet this specification.

The front-end amplification module features 4 preamplifiers for signals received from the silicon pad detectors. The signals from the silicon strip detector are handled by an application-specific integrated circuit (ASIC) on the Data Acquisition Module. More details about the DAM can be found in section 1.5.3.

1.3.5 Data Acquisition Module

The Data Acquisition Module (DAM) is the brain of the payload system consisting of the electrical hardware and firmware required for the mission. The DAM is responsible for reading data from the EST, monitoring the status of several sensors throughout the data acquisition subassembly, and communicating this data to the rest of the payload. In addition to reading and communicating data, the DAM is also responsible for delivering power to each board and component involved in acquiring data from the EST. The DAM houses a Xilinx Spartan 6 Field-Programmable Gate Array (FPGA), responsible for the main data processing and communication from the EST, as well as the PSIROC ASIC, responsible for processing the outputs from the silicon strip detector. The DAM also houses several power converters responsible for providing power to all sections of the data acquisition subassembly. More details about the DAM can be found in section 1.5.2.

1.3.6 Power Distribution Module

The power distribution module (PDM) will accept and convert the power supplied by the HASP gondola to an acceptable voltage for the DAM. The PDM features monitoring circuits and a microcontroller to monitor the quality of power supplied through the EDAC connector using ADCs. The PDM is also the bridge to pass data from the DAM to HASP. More details can be found in section 1.5.1

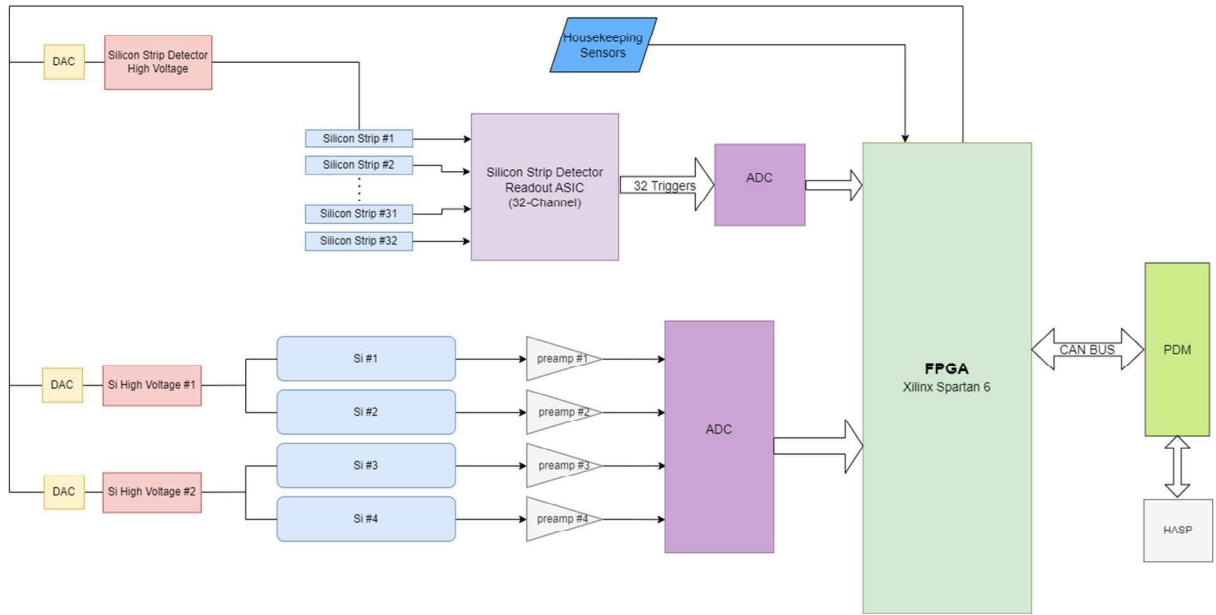


Figure 3 - System block diagram for the EST instrument

1.4 Mechanical and Structural Design

The structure of the 2023 HASP payload is similar to that of the previously flown mechanical structure by the team in 2021, enlarged to fit the large payload size. The assembly is made up of two identical rails held together by three structural trays positioned along the length of the rails. The EST is secured to the rails between the top and mid tray using twelve M3x0.5 screws. All of the mounting structure components are machined from Al 6061-T6. Each tray is connected to the rails using eight M3x0.5 ISO 10642 flat head screws. These fasteners thread into tapped holes in the trays with stainless steel coil wire inserts to reduce risk of fastener pullout. Primary fastener locking is achieved utilizing bolt preload with secondary locking provided by LOCTITE 242 threadlocker.

The payload is secured onto the provided mounting plate by eight M5 bolt and nut assemblies. Locking of the bolts is accomplished by the use of nylon-insert lock nuts secured on the backside of HASP payload plate. Serial connection and EDAC harnesses will be fed through a cutout on the bottom of the HASP student interface plate and connect to the Z- face of the PDM.

To verify the mechanical stresses seen by the payload during launch, multiple FEA studies will be conducted on the structure assembly. Experience in 5G and 10G shock simulations has been gained from the previous mission, NEUDOSE. Simulation of the previous structure resulted in a minimum factor of safety of 3.0 and the same standard will be upheld on PRESET.

1.5 Electrical Design

1.5.1 Power Distribution Module (PDM)

The PDM is responsible for monitoring and filtering the power received from HASP, as well as converting the received power to an acceptable voltage for the DAM and HVM. We will reuse the design of the PDM used on HASP 2021 on CNP-TEPC payload as it was proven to be a successful module. A block diagram of the power flow and electrical distribution system can be found in Figure 4 below.

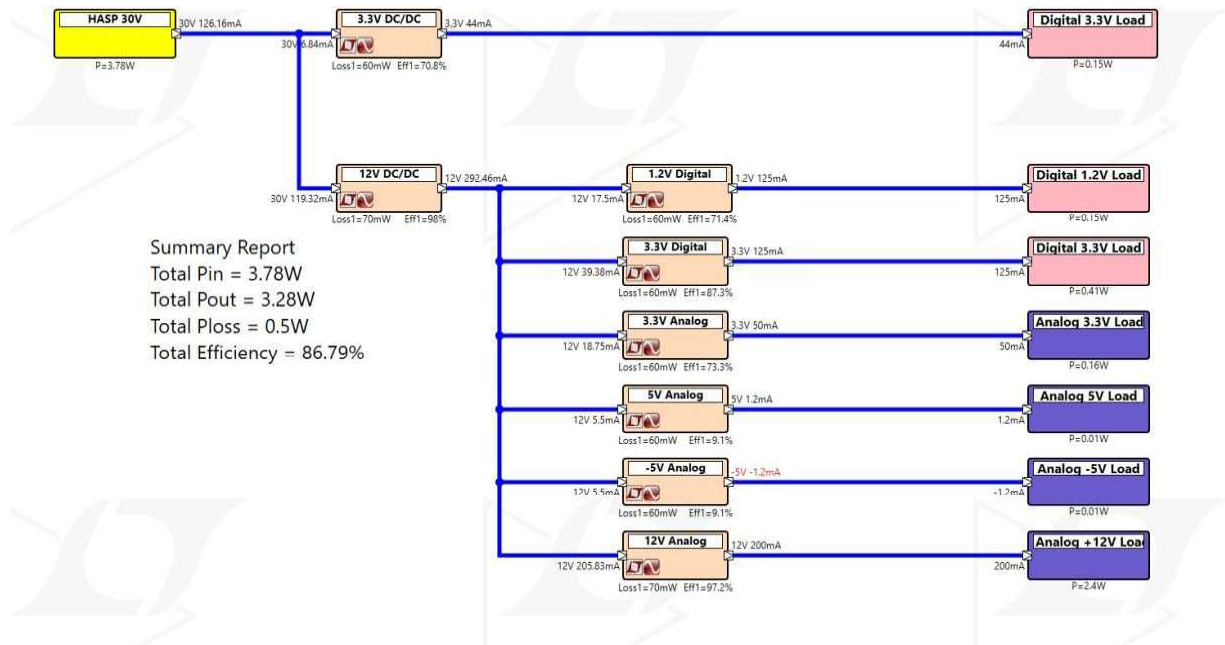


Figure 4 - Block diagram of the power flow and electrical distribution system.

The PDM uses two high efficiency LT8610 regulators to step down the +30V to +12V and +3.3V required by the EST and microcontroller on the PDM. The +12V power for the CNP-TEPC is then further converted on the DAM, discussed in section 1.5.4.

The payload will interface with HASP similarly to how it was interfaced with in the previous HASP 2021 missions. The pins from the EDAC connector that are to be used include the +30V power supply pins (A, B, C, D) and the ground pins (W, T, U, X). The DB9 connector will serve as the primary data port between the payload and HASP. The payload will utilize the Tx and Rx pins from the DB9 connector, grouping these two lines with the power and ground pins from the EDAC connector. Each of these lines will feed into a 6 pin T1SS Discrete Wire Cable (P/N T1SS-06-28-XX-08.0-X-XX). The four +30V wires will feed into two pins of the connector, with the four GND wires feeding into two different pins, with the Rx and Tx pins populating the last two pins. Each of the pins not in use will be capped off, labelled as no-connects.

Onboard the PDM is a microcontroller, responsible for monitoring the quality of the power supplied from HASP. The microcontroller will use ADCs to monitor the voltage and current values from the 3.3V and 12V power supplies, as well as monitor the voltage and current received from HASP. This monitoring system will also be used to characterize the inhibit switches. These switches will be mechanically opened and electrically closed. The switches will

be characterized individually by holding a known voltage across them while the microcontroller logs the current through them. The data will then be stored using the on-board flash memory which we can later analyze to see if they have misbehaved (electrically closed).

1.5.2 Data Acquisition Module (DAM)

The DAM houses 6 different power supplies to meet the power requirements for all components of the EST. The power supplies are separated into digital supplies (for digital components) and analog supplies (for analog components). The LTM4619 power converters are used to create the power for digital components for the EST. The LTM4619s produce 1.2V and 3.3V used for all digital components on the DAM (ADCs, Spartan 6 FPGA, Memory, etc.). The power requirements for the analog components are created from four LTM8045 converters that output 3.3V, 5V, -5V and 12V. Analog components include all components responsible for data acquisition, including components in the TEPC front end electronics, signal filtering and amplification, PSIROC analog components, and the High Voltage Power Supply. Each of the analog power supplies are not powered by default when the payload is applied power. The analog converters must be pulled up through an enable signal from the FPGA to be turned on.

All power converters on the DAM receive 12V from the PDM via a single connector. This 12V power is supplied by the PDM's own LT8610 power converters, converting the 30V from HASP.

The DAM interfaces with the PDM via a single 10 pin Molex connector. On this connector, there are:

- 2 pins for power
- 2 pins for GND
- 2 pins for CAN bus (One positive pin, one negative)
- 2 pins for RS232 communication (Rx and Tx)
- 2 pins unpopulated

Similar to the previous HASP 2021 mission, the DAM will be utilizing the RS232 as the main form of communication between the payload and HASP. The RS232 Rx and Tx signals will originate on the DAM through the usage of a MAX3221 integrated circuit, with the signals transmitted through the PDM to the HASP DB9 connection.

Spartan 6 FPGA

The Spartan 6 FPGA is the main processor used on the DAM and is responsible for processing all acquired data, preparing it for transmission to the HASP flight computer, monitoring temperatures, currents, voltages and pressures, as well as controlling all other settings of the payload that are able to be modified. The Spartan 6 monitors and controls each of the electronic components involved in the EST through firmware developed specifically for data acquisition and monitoring. The uploaded firmware on the FPGA processes acquired data, controls specific instrument settings, as well as communicates all data through the use of several data handlers.

The Spartan 6 is selected for this mission due to its proven tolerance to high levels of radiation as well as wide range of operating temperatures.

PSIROC

Another main component of the DAM is the PSIROC, used specifically for controlling and reading out the acquired data from the silicon strip detectors. Weeroc's PSIROC is a 64-channel ASIC designed for silicon diode and strip detector readout. In our application, only 32 channels will be used. Each input channel features a preamplifier, low/high gain sharper, peak detector and fast shaper. The adjustable shaping time and dual energy gain design provided great versatility and flexibility. It comes with a BGA package which makes implementation much easier. 64 analogue trigger outputs or 2 multiplexed outputs can be fed to an external analog-to-digital converter (ADC) for digitization and then pass to the FPGA for signal processing.

The output from PSIROC will be processed together with the signal from the front-end amplification module. Signals from PSIROC indicate particles entering the first silicon strip detector and trigger the coincidence logic in the FPGA firmware.

Housekeeping

The housekeeping section on the DAM are responsible for monitoring the voltage, current, temperature and pressure through the various sensors on the EST. Those sensors connected to three ADCs. These inputs are digitized in ADCs and sent via SPI to the FPGA.

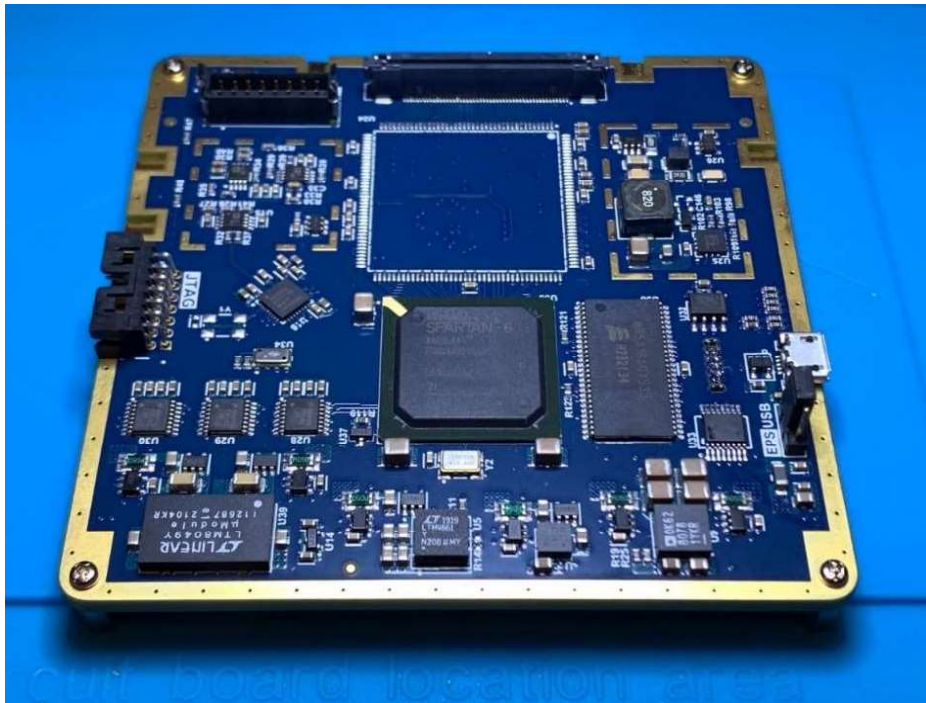


Figure 5 - Photograph of the data acquisition module (DAM) developed for the CNP-TEPC instrument on the NEUDOSE CubeSat mission. The analog section of the DAM will be modified for the EST instrument and made it to fit with PSIROC ASIC.

1.5.3 EST Electronics

Two of the major electric components involved with the EST are the High Voltage Module (HVM) and the Front-end Amplification Module (FAM), each of which are discussed in detail below.

EST High Voltage Module

The High Voltage Module (HVM), located directly below the silicon detector stack, is a PCB tasked with converting input voltage of +5V from the DAM into a high positive voltage to bias the silicon detectors. There are two types of silicon detectors, the EE2 silicon strip detector which require 75V to be fully depleted and the MSD040 single area silicon detector which requires 300V to reach full depletion.

A compact digital controlled regulator (MAX1932) from Analogy Device Inc. has been chosen to be the power supply for the EE2 silicon strip detector. MAX1932's output range is up to 90 V using a +5 V input from the DAM. The maximum current at 90 V is 2.5 mA. Output voltage can be programmed using its internal DAC controlled by the FPGA.

A miniature high voltage biasing supply made by Advanced Energy (0.5US5-P0.1) can produce a voltage range from 0V to -500V from an input voltage of 5V provided by the analog power converters on the DAM. The HV supply produces 0.1W of power, with a total current draw of 0.2 mA. The HV power supply has an adjustment voltage pin to control the output voltage leading to the silicon pad detectors. Two 0.5US5-P0.1 will be on the HVM as each one bias two cathode-to-cathode MSD040 detectors.

The MAX1932 output voltage can be directly program by the FPGA via SPI to the internal DAC. The 0.5US5-P0.1 high voltage output is determined by an input voltage adjustment compared with a reference voltage of +5V. This voltage adjustment value is set by a circuit on the DAM via a digital to analog converter. This voltage adjustment value is set by the FPGA, which is transmitted to a DAC via SPI. The DAC translates this transmitted voltage into an analog voltage value comparable to the High Voltage power supply's reference voltage. The output voltage is then connected back to the high voltage power supply where it is compared with the reference voltage.

Power Startup Sequence

When power is applied to the payload subsystem, the High Voltage Module is not powered, preventing any risk of shock. The HVM on/off state is controlled by the +5V analog power supply. The analog power supply is controlled by the Spartan 6 onboard FPGA. By default, when the payload is supplied power, the +5V analog regulator is not powered. To enable this regulator, the FPGA must send a high signal, which will eventually turn on the HVM. Due to this configuration, there is no risk of the HVM having power supplied to it when the power cable is connected, therefore eliminating the risk of electric shock.

EST Front-end Amplification Module

The electronic signal from a silicon detector is quite small and therefore requires multiple stages of amplification before being digitized. The most sensitive part of this process is the pre-amplification stage which collects the charges produced from radiation interactions in the silicon crystal. The EST Front-end Amplification Module (FAM) is responsible for this pre-amplification stage. Signals from each silicon pad detector are read using a Cremat CR111 charge sensitive preamplifier on the FAM and then fed to a high-speed ADC for digitization. There are 4 CR111 preamplifiers on the FAM. The CR111 preamplifier powered by ± 5 V generated from the DAM. The FAM is housed within the detector housing near the HVM.

1.6 Thermal Control Plan

The flight duration of up to 20 hours means the flight may extend into the night, meaning two steady-states conditions may be reached, with and without significant solar radiation. To gain an understanding of the temperature ranges the payload is expected to experience during this mission, two preliminary steady-state thermal simulations (a hot case and a cold case) were conducted with COMSOL software.

A brief overview of the simulation conditions follows. It is assumed the payload will experience no convective heat transfer, as ambient pressures of 5-10mbar are expected. The payload was geometrically simplified and is composed of materials including anodized Aluminum 6061-T6 and 304L stainless steel for structural components, and FR-4 and Silicon for PCB and solar boards. It is assumed the initial temperature for both cases is 293.15K, and the ambient temperature of the atmosphere is 230.15K. The former did not prove critical to the final resulting temperatures, while the latter is approximate of the typical ambient outside temperature on a previous mission. The final temperature range of the cold case is especially sensitive to modifications in the ambient temperature. Both the hot and cold cases include heat-emission from PCB components. Select outer boundaries for the hot case had a constant heat flux of 1361W/m^2 to represent solar radiation, while the cold case did not.

The hot case spans a temperature range of 278K ($\sim 5^\circ\text{C}$) to 325K ($\sim 52^\circ\text{C}$), which fits well within the operational temperature range of -20°C to 85°C for the most intolerant components of the payload. The cold case spans a significantly narrower temperature range of 231.5K ($\sim -41.5^\circ\text{C}$) to 236.5K ($\sim -37^\circ\text{C}$). This range is slightly above that of the operational temperature minimum (-40°C) for the EST and HVM but thermal solutions to increase the minimum temperature will be considered. Current simulations do not include thermal management solutions such as heat pipes, insulation, and thermal coatings. Future simulations will include these thermal solutions to better represent the physical instrument.

2. Team Structure and Management

2.1 Team Management

Benjamin Dyer will act as the student team leader, where his management duties include submission of monthly status reports, attending and documenting teleconference calls, documentation, and liaising between the student group and the 3 faculty and industry advisors.

Xingzhi Cheng and Benjamin Dyer will co-lead the instrument team. Their duties focus on the development, integration, and testing of the EST along with coordinating with other teams.

Leading the mechanical structure team is Patrick Chin. His duties include the design, construction, and integration of the payload structure. Mr. Chin will ensure the appropriate interfacing of all components of the payload.

Graham Power leads the firmware team. His duties include the design, testing, and integration of payload firmware, including the packet structure and development of register files.

The project will receive guidance and funding from 3 faculty and industry advisors who will also be in communication with the group on a weekly basis. The 3 advisors are:

- Dr. Andrei R. Hanu, a senior scientist at the Bruce Power Nuclear Generating Station and an adjunct assistant professor in the Department of Physics & Astronomy at McMaster University. Dr. Hanu developed the EST instrument and PRESET mission concepts and will provide guidance pertaining to the development of the mission and the science instrument.
- Dr. Soo-Hyun Byun, a professor in the Department of Physics & Astronomy at McMaster University. Dr. Byun will provide technical and theoretical guidance pertaining to the science instrument development.
- Dr. Eric Johnston, the chief innovation officer at the Nuclear Innovation Institute, a former HASP program student, and a co-principal investigator on the McMaster NEUDOSE mission.

2.2 Team Organization and Roles

The PRESET-EST team is composed of 10 students and 3 faculty advisors. The structure of the team is summarized in Table 1.

Table 1 - HASP team members, roles, and student statuses

NAME	ROLE	STUDENT STATUS	CONTACT
Benjamin Dyer	Student Project Lead, Instrument co-lead	Physics, PhD	dyerbm@mcmaster.ca
Xingzhi Cheng	Instrument co-lead	Medical Physics, PhD	chengx4@mcmaster.ca
Larysa Duda	Instrument Scientist	Medical Physics IV	dudal@mcmaster.ca

Connor Chandran	Instrument Scientist	Electronic Engineering and Management V	chandrac@mcmaster.ca
Patrick Chin	Mechanical Lead	Mechanical Engineering, PhD	chinpm@mcmaster.ca
Adam Tosti	Mechanical Team	Mechanical Engineering IV	tostia@mcmaster.ca
Conor Juárez	Mechanical Team	Mechanical Engineering III	oreilc1@mcmaster.ca
Graham Power	Firmware Lead	Mechatronics Engineering IV	powerg@mcmaster.ca
Michael Shi	Firmware Team	Engineering III	shim34@mcmaster.ca
Shyam Tanna	Firmware Team	Engineering III	tannas4@mcmaster.ca

The student group regularly meets on a weekly basis and also confers with at least one advisor once a week. In addition, the team maintains active communication and consistent documentation through web interfaces such as Slack and Confluence.

It is anticipated that 10 members and 2 advisors will attend integration and testing at the CSBF in 2023. The same 12 individuals are expected to participate in flight operations at Ft. Sumner in 2023.

2.3 Timeline and Milestones

The PRESET-EST team has identified four stages to complete before HASP 2023: design, fabrication, integration & testing, and flight of the mission. Each phase and its expected duration, as well as key milestones, are outlined in table 2. A full Gantt chart of the mission schedule can be found in Appendix A.

Table 2 - Phases of the PRESET mission, key milestones, and anticipated durations.

Phase/Milestone	Date(s)	Description
Phase A: Design	Sep. 2022-Apr. 2023	Design of all physical components. Development of all electronic systems for the EST, PDM, and DAM.
Mechanical Design Review	Mar. 2023	Finalization of mechanical design
Electronics Design Review	Apr. 2023	Finalization of electronics design
Phase B: Fabrication	Feb. - May. 2023	Ordering, fabrication, and inspection of all components
Preliminary PSIP Document Due	Apr. 2023	Preliminary document of specification and integration plan
NASA Integration On-Site Security Document due	Apr. 2023	Document for on-site access at the CSBF

Phase C: Integration & Testing	Feb. - Aug. 2023	Integration of components into housing, thermal vacuum, vibration/shock and radiation testing. Instrument calibration and integration at CSBF.
Final PSIP Document Due	June. 2023	Final document of specification and integration plan
NASA Flight On-Site Security Document Due	Jun. 2023	Document for on-site access at HASP launch
Final FLOP Document Due	Jul. 2023	Final document of flight operation plan
Phase D: Flight and End of Mission	Sep. - Nov. 2023	Flight preparation operations. Recovery, packing and returning payload. End of mission documentation.

2.4 Anticipated Participation in Integration and Launch operations

The EST has been designed for autonomous operation and minimal operations during integration and throughout flight is expected. During integration, we require the payload to be bolted to the mounting plate and the serial and power connectors to be attached. All other assembly of the payload will be done prior to integration with the HASP balloon. We anticipate the following steps for successful payload integration:

- Provide the latest payload mechanical and electrical interface control documents.
- Pre-integration inspection to confirm HASP compliance (mass, voltage, and current)
- Test instrument power up using HASP bench test hardware
- Test instrument telemetry using HASP bench test hardware
- Mount instrument to HASP platform
- Test instrument power up using actual HASP flight hardware
- Test instrument telemetry using actual HASP flight hardware
- Perform pre-flight thermal vacuum testing
- Test instrument communications throughout flight. Verify with HASP interface

During flight, the EST will operate autonomously and send a full dataset using the serial downlink every 10 minutes.

3. Payload Interface Specifications

3.1 Weight Budget

The weight budget for the payload is presented in Table 3. The total weight of the payload has been calculated to be 2.209 ± 0.214 kg. A 10% margin of error was included for each component. The mass of the mechanical subsystem was increased 100% from the HASP 2021

mission to account for moving from a small to large payload. The payload weight is well within the 20kg allocated to large payloads.

Table 3 - Weight budget for the HASP 2023 PRESET mission.

Item	Mass (g)	Uncertainty (g)	Comments
Mechanical Subsystem	1000	100	Based on mass of HASP 2021 mechanical system
EST	1000	100	Based on CAD estimate
Data Acquisition Module	68	2	Measured mass of current module
Power Delivery Module	71	2	Measured mass of manufactured module
Front End Amplification Module	70	10	Based on CAD estimate
TOTAL	2209	214	

3.2 Power Budget

For the HASP 2023 mission we are sending the EST assembly and power distribution module. In total this creates a peak power draw of 2.278W which is well within the 75W allotment for large payloads. The ~2.3W power draw is primarily from the EST and supporting electronics, while 0.143W is allocated to the power delivery module. Table 4 shows the expected power draw for each payload component.

Table 4 - Power consumption values for the HASP 2023 PRESET mission.

Item	Voltage	Current(mA)	Power (W)	Comments
Front End Amplification Module	+/-5V	60±5	0.3	Based on manufacturer estimates
High Voltage Module	+12V	80±5	0.6	Based on preliminary testing
Power Delivery Module	+30V	44±3	0.143	Based on HASP 2021 testing
Data Acquisition Module	+12V	103±10	1.235	Based on testing of current module
TOTAL			2.278	

The current draw in the high voltage module is a worst-case scenario where the detectors are always fully saturated. During operation, the detector current is expected to be less than 10uA resulting in a projected high voltage module power draw of 0.05W. Additionally, the high voltage module will only operate once altitude is reached and will be disabled before descent. The power usage in this table is based off the worst-case scenario with all components drawing maximum power.

3.3 Downlink Serial Data

The EST payload produces two spectra every 5 minutes. The spectra are the main data product and are stored as 2-byte values in 50 bins resulting in 100 bytes per measurement interval. Including 12 start and stop bytes, each data set will include 86 bytes of "housekeeping" data, 2 GPS measurements at 125 bytes each, and 2 bytes of XOR Redundancy Check information, making each transmitted file 350 bytes in size. Due to low count rates, the trace data will also be transmitted. The expected maximum counting rate is 5 events/second, with each event producing five 2-byte energy values, a 4-byte time value, and a 1-byte particle type value. The trace data will be transmitted once a second. Including 12 start and stop bytes results in a maximum trace data rate of 82 bytes/s. Using the 8-N-1 encoding scheme, the required downlink will be $122 \text{ bytes/s} \cdot 9/8 \cdot 8 \text{ bits/1 byte} = 1098 \text{ bits/s}$ which falls within the upper limit of 4800 bps allocated to large payloads. Histogram and trace data will also be stored locally on the payload to test the data storage and recovery capabilities of the EST.

3.4 Uplink Serial Commanding

We intend to use the serial uplink, but all commands will be kept under the two byte limit. Serial commands to toggle the radio on and off will be utilized.

3.5 Analog Downlink

We will not be using analog downlink.

3.6 Discrete Commanding

We will not be using discrete commanding.

3.7 Payload Location and Orientation Request

While the proposed payload fits within the budgets of a small payload, we have requested a large payload seat to mitigate the risk of breaking the silicon detectors. The detectors used in the EST are both fragile and expensive but must be exposed directly to the outside environment through the collimator. We have requested a large payload seat to reduce the risk of the payload being the principal point of contact on landing. Additionally, the location of the large payload seats ensures the instrument will not be dragged along the ground where the protective shutter could be damaged exposing the detectors to dust and debris.

3.8 Special Requests

The EST uses one item on the Hazardous Materials List, a high voltage module. The HVM is a modification of the previous module flown on HASP missions in 2017, 2018, and 2021. The HVM is mounted to the base of the EST, directly beneath the front-end amplification module. The HVM supplies 0-500V to the silicon detectors located within the EST. This is critical to the EST operation as the silicon detectors must be reversed biased until they have reached full depletion. Testing of the silicon detectors has shown full depletion occurs at 300V for the

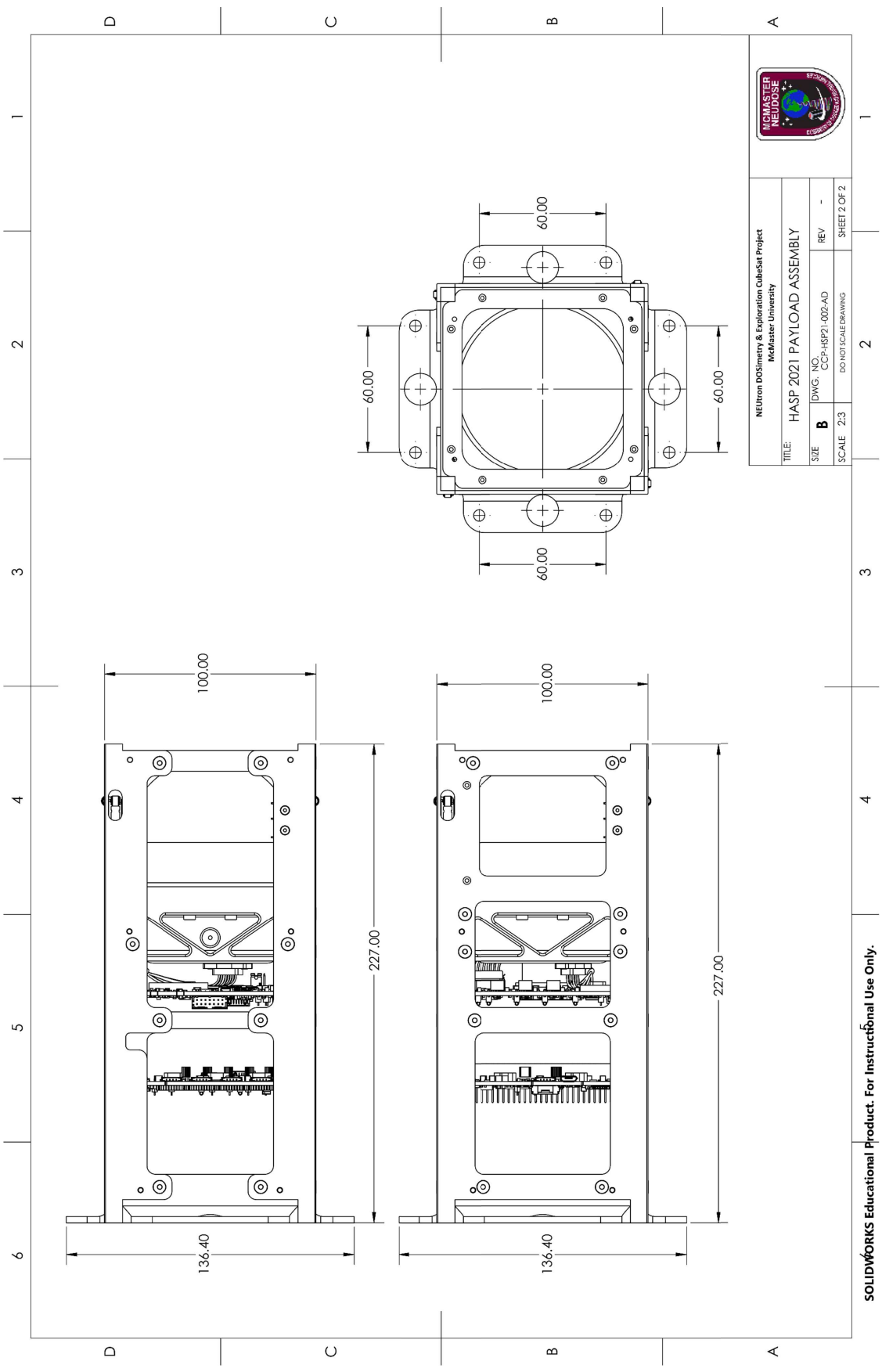
1500um thick detectors and at 75V for the 500um thick detector. Due to the startup sequence configuration and the grounding of the HVM, we do not expect any safety concerns when handling the EST.

4. Preliminary Drawings and Diagrams

The mechanical structure and mounting method will be minor adjustments from the HASP 2021 mission. Attached are drawing and photos of components which will be reused with minor modification for the HASP 2023 mission. Of particular interest is the mounting plate which will be enlarged to fit the large payload mount.



Figure 6 - PCB top of the DAM, fabricated December 2020.

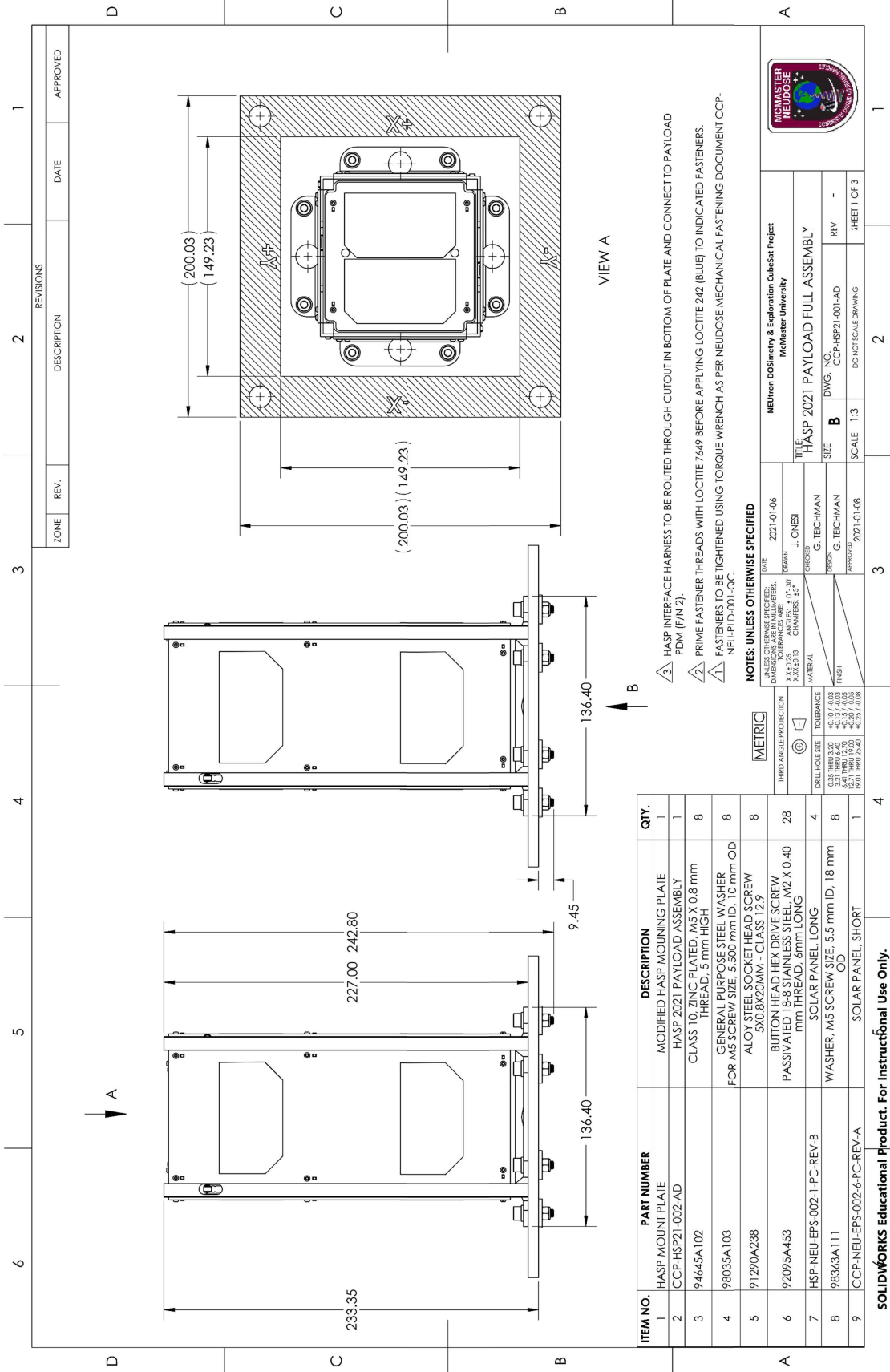


NEUtron DOSimetry & Exploration CubeSat Project
McMaster University

TITLE: HASP 2021 PAYLOAD ASSEMBLY

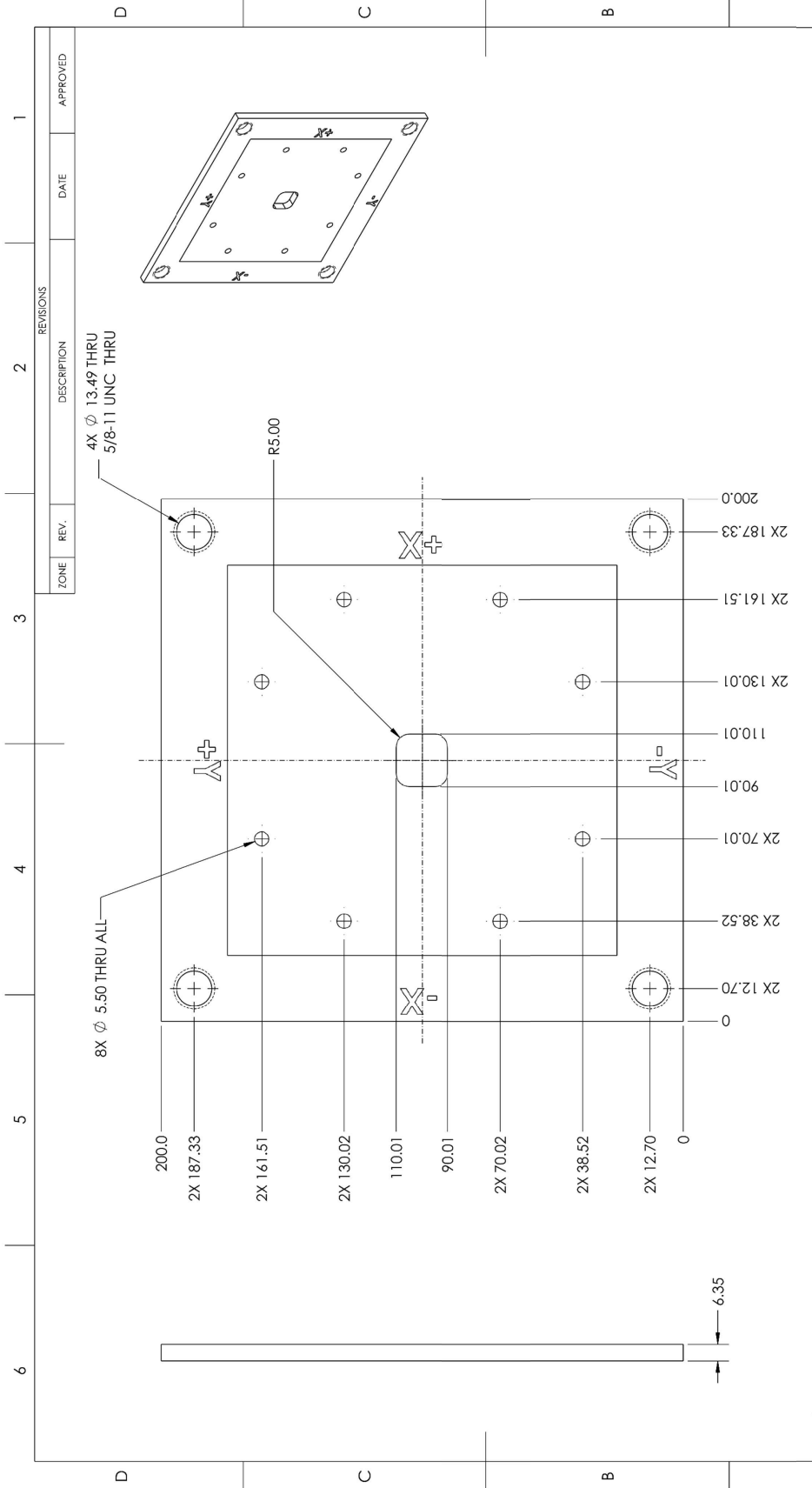
SIZE	DWG. NO.	REV
B	CCP-HSP21-002-AD	-

SCALE: 2:3
DO NOT SCALE DRAWING
SHEET 2 OF 2



ITEM NO.	PART NUMBER	DESCRIPTION	QTY.
1	HASP MOUNT PLATE CCP-HSP21-002-AD	MODIFIED HASP MOUNTING PLATE HASP 2021 PAYLOAD ASSEMBLY	1
2	94645A102	CLASS 10 ZINC PLATED, M5 X 0.8 mm THREAD, 5 mm HIGH	8
3	98035A103	GENERAL PURPOSE STEEL WASHER FOR M5 SCREW SIZE, 5.500 mm ID, 10 mm OD	8
4	91290A238	ALLOY STEEL SOCKET HEAD SCREW 5X0.8X20MM - CLASS 12.9	8
5	92095A453	BUTTON HEAD HEX DRIVE SCREW PASSIVATED 18-8 STAINLESS STEEL, M2 X 0.40 mm THREAD, 6mm LONG	28
6	HSP-NEU-EPS-002-1-PC-REV-B	SOLAR PANEL, LONG	4
7	98363A111	WASHER, M5 SCREW SIZE, 5.5 mm ID, 18 mm OD	8
8	CCP-NEU-EPS-002-6-PC-REV-A	SOLAR PANEL, SHORT	1

SOLIDWORKS Educational Product. For Instructional Use Only.



FINISH: NONE MATERIAL: N/A 1. DIMENSIONAL LIMITS APPLY AFTER Δ NOTES:		THIRD ANGLE PROJECTION DRILL HOLE SIZE TOLERANCE 0.35 THRU 0.30 +0.10 / 0.03 0.41 THRU 0.50 +0.13 / 0.05 0.51 THRU 0.75 +0.20 / 0.08 0.76 THRU 1.00 +0.27 / 0.08 1.01 THRU 2.00 +0.35 / 0.08		METRIC UNLESS OTHERWISE SPECIFIED, DIMENSIONS ARE IN MILLIMETERS. X.34/25 ANGLES: 01:50° X.40/25 CHAMFERS: 5°		DATE: 12-16-2020 DRAWN: ONESI CHECKED: DESIGNED: APPROVED:		NEUTRON DOSEIMETRY & Evaluation CubeSat Project Acute per University	
TITLE: HASP MOUNTAIN PLATE		SIZE: B		SCALE: 3:4		REV: -		SHEET: 1 OF 1	
ZONE:		REV.:		DESCRIPTION:		DATE:		APPROVED:	



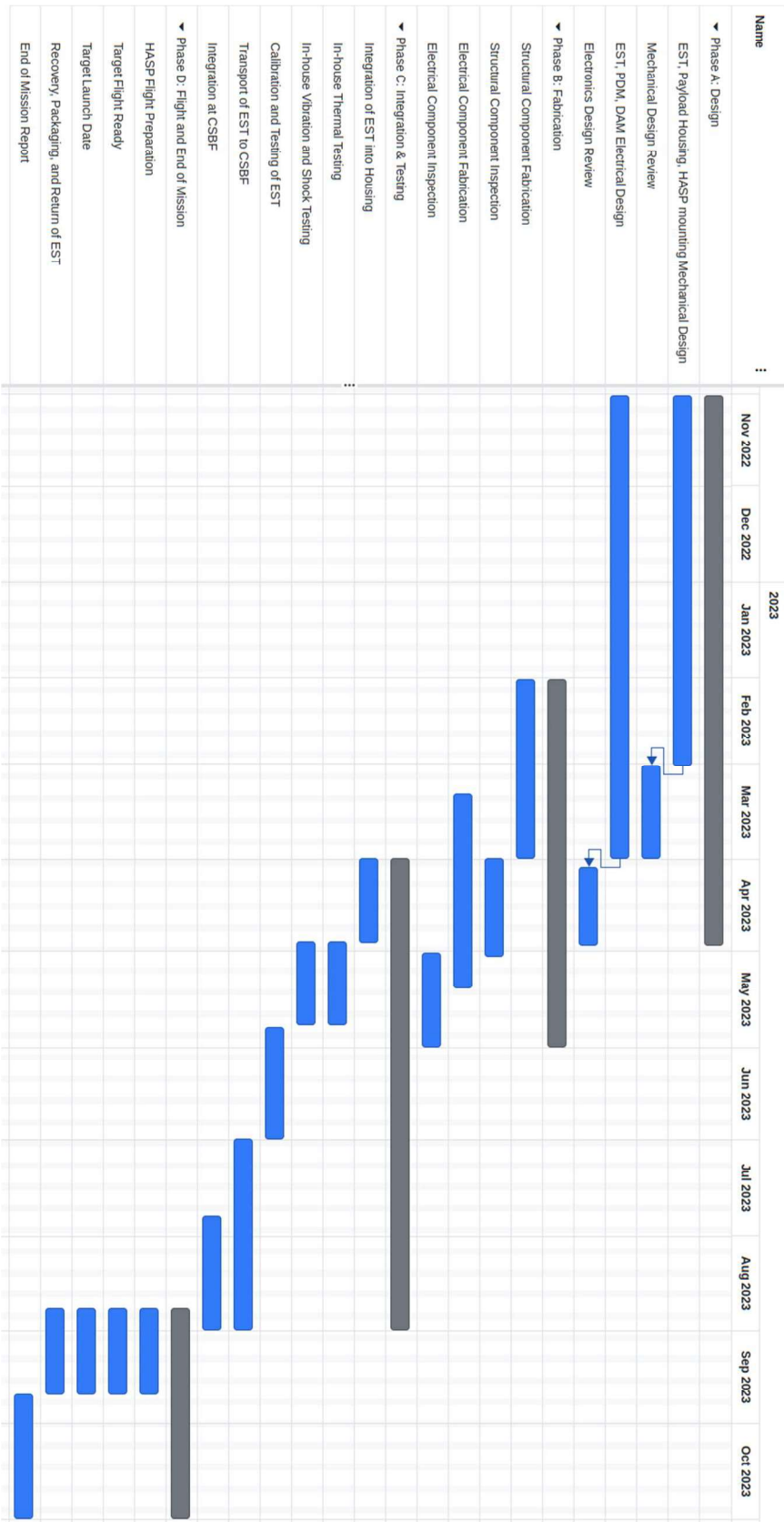
SOLIDWORKS Educational Product. For Instructional Use Only.

5. References

- [1] A. Hanu, J. Barberiz, D. Bonneville, S.H. Byun et al., NEUDOSE - A CubeSat mission for dosimetry of charged and neutral particles, *Radiat. Res.* 187 (2017) 42-49.
- [2] A. Barovier, D. Wagner, W. Ward, A.R. Hanu, E. Johnston, S.H. Byun, Passive attitude control to decrease CubeSatellite complexity, 2020 Small Satellite Conference, August 1-6, 2020, Utah State University, USA.
- [3] J. Nguyen, S.H. Byun, W. Donaldson, A.R. Hanu et al., Architecture and design of the McMaster NEUDOSE communication radio subsystem, 2020 Small Satellite Conference, August 1-6, 2020, Utah State University, USA.
- [4] M. Ayesh, J. Barberiz, P. Bosca, A. Bruinsma, S.H. Byun et al., Design of a custom secondary on-board computer for the NEUDOSE CubeSat mission, 2020 Small Satellite Conference, August 1-6, 2020, Utah State University, USA.
- [5] National Academies of Sciences, Engineering, and Medicine. 2020. Progress Toward Implementation of the 2013 Decadal Survey for Solar and Space Physics: A Midterm Assessment. Washington, DC: The National Academies Press. <https://doi.org/10.17226/25668>.
- [6] Zong, Q., Wang, Y., Yuan, C. et al. Fast acceleration of “killer” electrons and energetic ions by interplanetary shock stimulated ULF waves in the inner magnetosphere. *Chin. Sci. Bull.* **56**, 1188–1201 (2011). <https://doi.org/10.1007/s11434-010-4308-8>
- [7][25] Andersson, M., Verronen, P., Rodger, C. *et al.* Missing driver in the Sun–Earth connection from energetic electron precipitation impacts mesospheric ozone. *Nat Commun* **5**, 5197 (2014). <https://doi.org/10.1038/ncomms6197>
- [8] Clem, K.R., Renwick, J.A. & McGregor, J. Relationship between eastern tropical Pacific cooling and recent trends in the Southern Hemisphere zonal-mean circulation. *Clim Dyn* **49**, 113–129 (2017). <https://doi.org/10.1007/s00382-016-3329-7>
- [9] Lim, E.-P., Hendon, H. H., Arblaster, J. M., Delage, F., Nguyen, H., Min, S.-K., and Wheeler, M. C. (2016), The impact of the Southern Annular Mode on future changes in Southern Hemisphere rainfall, *Geophys. Res. Lett.*, 43, 7160– 7167, doi:[10.1002/2016GL069453](https://doi.org/10.1002/2016GL069453).
- [10] Kostov, Y., Marshall, J., Hausmann, U. *et al.* Fast and slow responses of Southern Ocean sea surface temperature to SAM in coupled climate models. *Clim Dyn* **48**, 1595–1609 (2017). <https://doi.org/10.1007/s00382-016-3162-z>
- [11] Oliveira, F.N.M. and Ambrizzi, T. (2017), The effects of ENSO-types and SAM on the large-scale southern blockings. *Int. J. Climatol.*, 37: 3067-3081. <https://doi.org/10.1002/joc.4899>
- [12] Barnes, P.W., Williamson, C.E., Lucas, R.M. *et al.* Ozone depletion, ultraviolet radiation, climate change and prospects for a sustainable future. *Nat Sustain* **2**, 569–579 (2019). <https://doi.org/10.1038/s41893-019-0314-2>
- [13] Semeniuk, K., Fomichev, V. I., McConnell, J. C., Fu, C., Melo, S. M. L., & Usoskin, I. G. (2011). Middle atmosphere response to the solar cycle in irradiance and ionizing particle precipitation. *Atmospheric Chemistry and Physics*, **11**(10), 5045– 5077.
- [14] Codrescu, M. V., Fuller-Rowell, T. J., Roble, R. G., and Evans, D. S. (1997), Medium energy particle precipitation influences on the mesosphere and lower thermosphere, *J. Geophys. Res.*, 102(A9), 19977– 19987, doi:[10.1029/97JA01728](https://doi.org/10.1029/97JA01728).
- [15] Arsenovic, P., Rozanov, E., Stenke, A., Funke, B., Wissing, J., Mursula, K., et al. (2016). The influence of middle range energy electrons on atmospheric chemistry and regional climate. *Journal of Atmospheric and Solar-Terrestrial Physics*, **149**, 180– 190.

- [16] Meraner, K., & Schmidt, H. (2018). Climate impact of idealized winter polar mesospheric and stratospheric ozone losses as caused by energetic particle precipitation. *Atmospheric Chemistry and Physics*, **18**(2), 1079– 1089. <https://doi.org/10.5194/acp-18-1079-2018>
- [17] Tyssøy, H. N., Haderlein, A., Sandanger, M. I., & Stadsnes, J. (2019). Intercomparison of the POES/MEPED loss cone electron fluxes with the CMIP6 parametrization. *Journal of Geophysical Research: Space Physics*, **124**, 628– 642. <https://doi.org/10.1029/2018JA025745>
- [18] Tyssøy, H.N., Sadanger, M. I., Ødegaard, L.-K.G., Standsnes, J., Aasnes, A., Zawedde, A. E., Energetic electron precipitation into the middle atmosphere – Constructing the loss cone fluxes from MEPED POES. *Journal of Geophysics Research: Space Physics*. **121**(6), 5693-5707 (2016). <https://doi.org/10.1002/2016JA022752>
- [19] Stratton, J.M., Harvey, R.J. & Heyler, G.A. Mission Overview for the Radiation Belt Storm Probes Mission. *Space Sci Rev* **179**, 29–57 (2013). <https://doi.org/10.1007/s11214-012-9933-x>
- [20] Bakr, D.N., Kanekal, S.G., Hoxie, V. et al. The Relativistic Electron-Proton Telescope (REPT) Investigation: Design, Operational Properties, and Science Highlights. *Space Science Reviews* **217**, 68 (2021). <https://doi.org/10.1007/s11214-021-00838-3>
- [21] Mitani, T., Takashima, T., Kasahara, S. et al. High-energy electron experiments (HEP) aboard the ERG (Arase) satellite. *Earth Planets Space* **70**, 77 (2018). <https://doi.org/10.1186/s40623-018-0853-1>
- [22] Kasahara, S., Miyoshi, Y., Yokota, S. et al. Pulsating aurora from electron scattering by chorus waves. *Nature* **554**, 337–340 (2018). <https://doi.org/10.1038/nature25505>
- [23] T. Sato. EXPACS: Excel-based Program for calculating Atmospheric Cosmic-Ray Spectrum. Users' Manual. 2009

Appendix A: Timeline and Milestone WBS Documentation



Appendix B: NASA Hazard Tables

Appendix B.1 Radio Frequency Transmitter Hazard Documentation

HASP 2022 RF System Documentation	
Manufacture Model	N/A
Part Number	N/A
Ground or Flight Transmitter	N/A
Type of Emission	N/A
Transmit Frequency (MHz)	N/A
Receive Frequency (MHz)	N/A
Antenna Type	N/A
Gain (dBi)	N/A
Peak Radiated Power (Watts)	N/A
Average Radiated Power (Watts)	N/A

Appendix B.2 High Voltage Hazard Documentation

HASP 2022 High Voltage System Documentation	
Manufacture Model	0.5US5-P0.1
Part Number	633-0.5US5-P0.1-ND
Location of Voltage Source	EST detector housing
Fully Enclosed (Yes/No)	Yes
Is High Voltage source Potted?	Yes
Output Voltage	0-500 V
Power (W)	0.1 W
Peak Current (A)	0.2 mA
Run Current (A)	0.2 mA

HASP 2022 High Voltage System Documentation	
Manufacture Model	MAX1932
Part Number	MAX1932ETC+T
Location of Voltage Source	EST detector housing
Fully Enclosed (Yes/No)	Yes
Is High Voltage source Potted?	Yes
Output Voltage	4.5-90 V
Power (W)	0.1 W
Peak Current (A)	2.5 mA
Run Current (A)	1 mA

Appendix B.3 Laser Hazard Documentation

HASP 2022 Laser System Documentation			
Manufacture Model		N/A	
Part Number		N/A	
Serial Number		N/A	
GDFC ECN Number		N/A	
Laser Medium		N/A	
Type of Laser		N/A	
Laser Class		N/A	
NOHD (Nominal Ocular Hazard Distance)		N/A	
Laser Wavelength		N/A	
Wave Type		N/A	
Interlocks		N/A	
Beam Shape		N/A	
Beam Diameter (mm)	N/A	Beam Divergence (mrad)	N/A
Diameter at Waist (mm)	N/A	Aperture to Waist Divergence (cm)	N/A
Major Axis Dimension (mm)	N/A	Major Divergence (mrad)	N/A
Minor Axis Dimension (mm)	N/A	Minor Divergence (mrad)	N/A
Pulse Width (sec)	N/A	PRF (Hz)	N/A
Energy (Joules)	N/A	Average Power (W)	N/A
Gaussian Coupled (e-1, e-2)		N/A	
Single Mode Fiber Diameter		N/A	
Multi-Mode Fiber Numerical Aperture (NA)		N/A	
Flight Use or Ground Testing Use?		N/A	

Appendix B.4 Battery Hazard Documentation

HASP 2022 Battery Hazard Documentation	
Battery Manufacturer	N/A
Battery Type	N/A
Chemical Makeup	N/A
Battery modifications	<i>(Must be NO)</i>
UL Certification for Li-Ion	N/A
SDS from manufacturer	N/A
Product information sheet from manufacturer	N/A